SOLPS-ITER modeling of EU-DEMO Ar-seeded cases with drifts and kinetic neutrals

Korzueva V., Kaveeva E., Vekshina E., Rozhansky V., Senichenkov I., Shirobokov A., Coster D.

Abstract.

SOLPS-ITER modeling of EU-DEMO tokamak burning plasma with Ar seeding was performed. The modeling includes drifts, kinetic neutrals and current description switched on. Simulation results are compared with ones without drifts. Power entering the edge plasma domain is 200 MW. Deuterium puff is $1.5 \cdot 10^{23}$ $\frac{at}{s}$ for all cases, which corresponds to neutral deuterium pressure 10 Pa in the private flux region. Ar seeding rates are $8.0 \cdot 10^{19}$ $\frac{at}{s}$ and $1.5 \cdot 10^{20}$ $\frac{at}{s}$, which corresponds to argon concentration on the separatrix in the range of 0.5-2%. It's demonstrated that with such combination of parameters it's possible to achieve power loads lower than 5 MW/m^2 on both divertor targets. The temperature above 5 eV in the far SOL of the outer target still remains an issue. Along with drift and no drift comparison, impurity accumulation mechanism in the high field side SOL is discussed.

1. Introduction

According to EU-DEMO design predictions from Ref. [1], a large amount of its power must be radiated by impurity. This can help to decrease power flux density and electron temperature on divertor targets and prevent tungsten sputtering. Several publications, such as Ref. [2],[3], explore possible impurity seeding and deuterium puffing rates to achieve conditions with electron temperature and power flux density below 5 eV and $5MW \cdot\ m^{-2}$, respectively. Up to now such modeling for EU-DEMO was done without drifts or without kinetic neutrals.

According to SOLPS-ITER modeling of ITER from Ref. [4], despite the fact that drifts don't play such significant role in plasma and impurity redistribution as in smaller devices [5], power flux density and electron temperature are higher on the outer divertor target than corresponding values without drifts. The degree of such effect depends on the neutral deuterium pressure in the private flux region(PFR) of divertor and on the degree of detachment [4].

To model such effect carefully kinetic neutrals description should also be included in the simulation. Newest EU-DEMO SOLPS-ITER modeling with drifts and kinetic neutrals has demonstrated that it's possible to achieve electron temperature below 5 eV in strike-point vicinity with medium Ar seeding and high D puff [6]. The case is characterized with 20 Pa neutral deuterium pressure in the PFR.

This work presents EU-DEMO SOLPS-ITER modeling results that complement an argon seeded case presented in Ref. [6]. The work explores other possible Ar seeding rates with lower D puff in cases with and without drifts. Similarly to Ne in ITER, distribution of Ar in the EU-DEMO scrape off layer (SOL) is observed and described.

Neutral deuterium pressure for presented cases is about 10 Pa. All cases contain kinetic description of neutrals by Eirene with included neutral-neutral collisions.

2. Modeling setup

Fig. 1 shows a computational mesh for SOLPS-ITER modeling of EU-DEMO. D puff and Ar seeding are placed on the top of the vacuum vessel. This choice was discussed in the previous work [6]: if the gas is puffed from the outer midplane, it artificially increases neutral flux through the separatrix to the core region. Pump slots are at the bottom of the PFR. The dome structure is absent. The neutrals pressure in the PFR mentioned above is calculated at the boundary of blue and orange meshes.

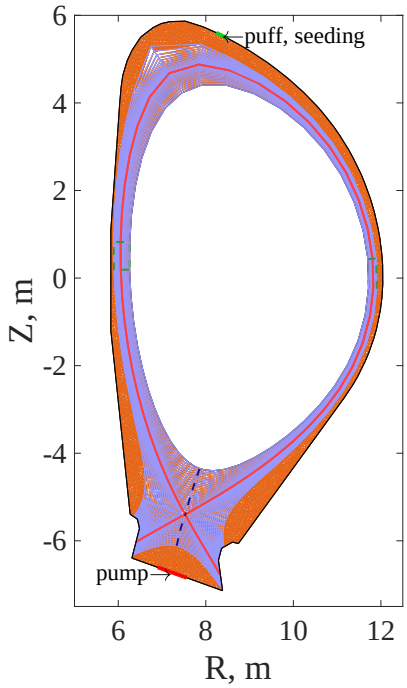

Figure 1. Computational mesh of EU-DEMO. The same as in Ref. [6].

Anomalous transport coefficients are presented in fig. 2. They remain the same as in the previous paper Ref. [6]. The decay length for modeled poloidal conductive electron heat flow at the outer divertor entrance [6] is in the range 2.3-2.7 mm.

Main ion density on the core boundary is fixed to $6 \cdot 10^{19}\ m^{-3}$, which corresponds to ASTRA modeling of EU-DEMO [7]. Plasma energy flux is 200 MW on the inner core boundary, equally shared between ions and electrons. $\Gamma_{He^{+2}} = 3.5 \cdot 10^{20}\ s^{-1}$ on the same boundary is set to match the 1 GW scenario.

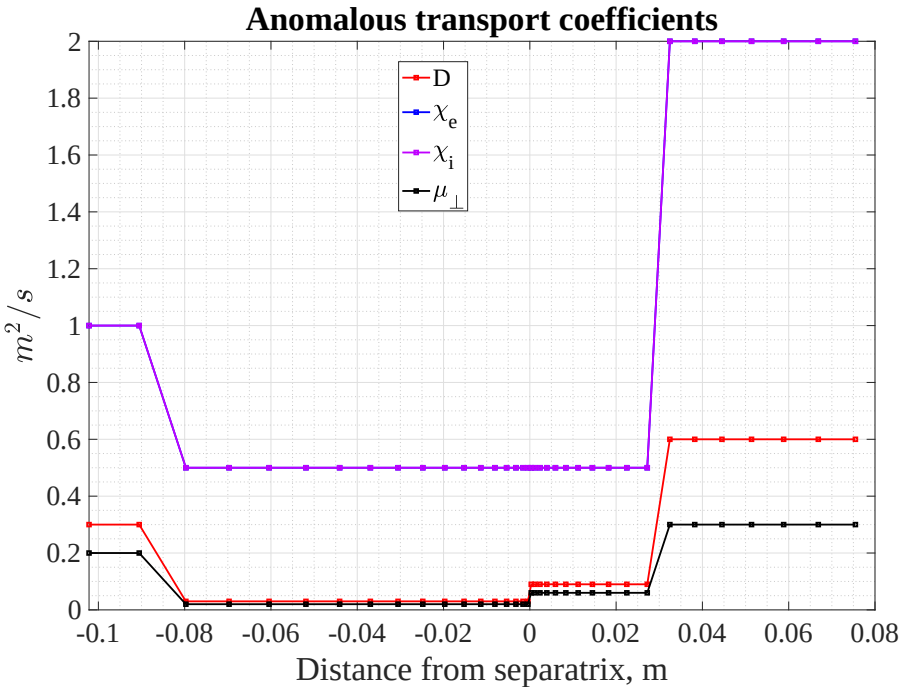

Figure 2. Coefficients of anomalous transport: diffusivity, electrons thermal conductivity, ions thermal conductivity, viscosity.

In this work a series of cases with different Ar seedings is presented. Each case is simulated both with and without drifts to investigate the exact impact of drifts. Parameters of cases are described in the table 1 along with that for the case from Ref. [6]. All simulations were performed using kinetic neutrals description by code Eirene with reactions and collision rates for atoms and D_2 the same as in Ref. [6].

The ionization and recombination rates for argon correspond to ADAS89 database. These rates are calculated in Coronal equilibrium limit and can underestimate the ionization for big electron density. According to [8] this can lead to underestimation of Ar compression in divertor. Still, for accurate conclusions devoted modeling is necessary with newest databases, ADAS96 or later.

3. Modeling results

3.1. Midplane profiles

Figures 3-5 contain modeling results for cases which meet the conditions of target heat load below 5 MW/m^2 with drifts compared with Ar seeded case from the previous work [6]. The main difference between the previous case and presented ones is neutral deuterium pressure. Presented cases have about $p_{D+D_2} = 10\ Pa$ (see table 1), while the previous published Ar case has $p_{D+D_2} = 20\ Pa$ [6].

Figure 3a shows main ions density distribution at the outer midplane. Main ions density at the separatrix varies from $1.7 \cdot 10^{19}\ m^{-3}$ to $2.8 \cdot 10^{19}\ m^{-3}$ in presented cases (except the case from Ref. [6]). Such values should be compatible with transport barrier

Table 1. Main parameters of modeled scenarios. The table contains: a case name (first left column), argon puff rate, deuterium puff rate, the neutral deuterium pressure in the PFR, the relative to deuterium concentration of Ar at the separatrix, the relative to deuterium concentration of He at the separatrix, peak outer target electron temperature, peak outer target power flux density, total radiated power as percent of power crossing the inner core boundary.

Name	Γ^{Ar}_{puff}, $10^{20}\frac{at}{s}$	Γ^{D}_{puff}, $10^{23}\frac{at}{s}$	p_{D+D_2}, Pa	c_{Ar}, %	c_{He}, %	T^{targ}_{max}, eV	q^{targ}_{max}, $\frac{MW}{m^2}$	Q_{rad}, %
1.5e20Ar_1.5e23D, drifts on	1.5	1.5	11	0.9	1.8	32	2.3	74
1.5e20Ar_1.5e23D, drifts off	1.5	1.5	12	2.1	7.7	20	2.0	75
0.8e20Ar_1.5e23D, drifts on	0.8	1.5	10.5	0.6	2.7	40	4.0	69
0.8e20Ar_1.5e23D, drifts off	0.8	1.5	11	0.5	6.4	22	3.5	67
0.4e20Ar_1.5e23D, drifts on	0.4	1.5	10.5	0.35	4.4	39	6.2	55
0.4e20Ar_1.5e23D, drifts off	0.4	1.5	10.5	0.23	3.9	21	5.4	59
0.8e20Ar_3.0e23D, drifts on, [6]	0.8	3.0	20	0.4	2.1	15	4.0	62

according to criterion from Ref. [9] of separatrix density below half of Greenwald limit. In runs without drifts the decrease of ions density with increase of seeding is clearly seen. It's associated with decrease of plasma pressure in the SOL due to increase of effective ionization cost. This effect was observed in experiments on existing tokamaks and in modeling from Ref. [4],[10],[11]. Interestingly, this effect is very small in runs with drifts.

Figures 3b shows electron temperature. Drift inclusion doesn't impact on electron temperature profiles inside the separatrix.

Figures 4 and 5a show effective charge and argon density at the outer midplane, respectively. Higher Ar density at the outer midplane is obtained in cases without drifts. Three of presented cases have higher argon presence in the high field side (HFS) SOL, see fig. 5b. Details on argon distribution are discussed in section 3.3.

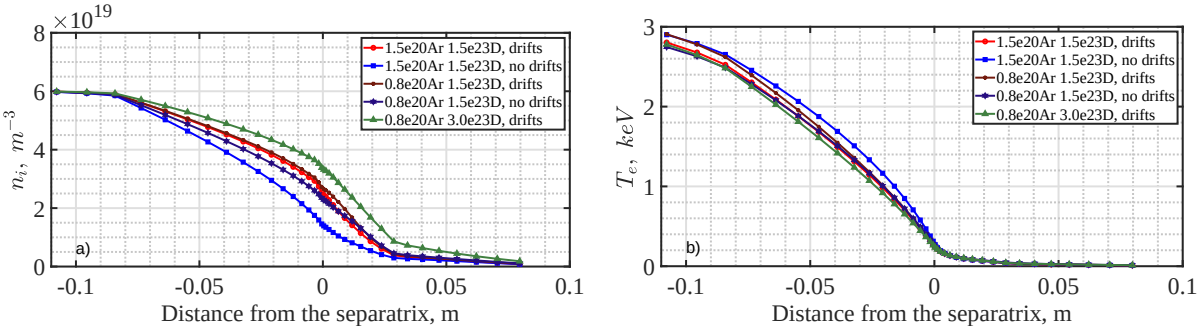

Figure 3. a) Main ion density and b) electron temperature at the outer midplane.

Helium and argon concentration averaged on the separatrix is described in the table 1. The helium concentration at the separatrix in all cases is below operational limits of NNN for EU-DEMO [NNN]. The standard SOLPS-ITER 3.0.7 model was used in the

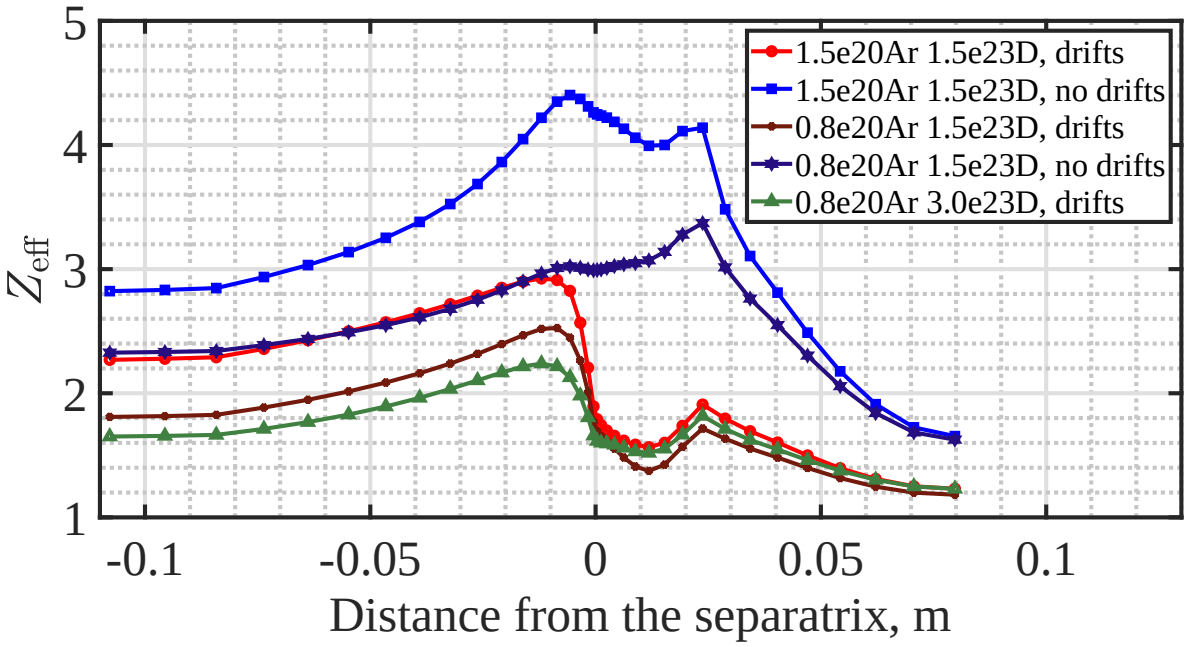

Figure 4. Effective charge density at the outer midplane.

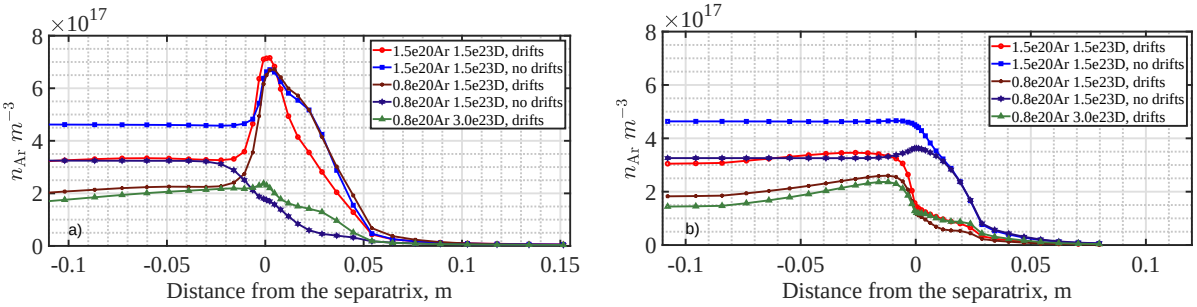

Figure 5. Argon ion density profiles a) at the inner midplane and b) at the outer midplane.

simulation for kinetic coefficients (parallel friction and thermal force between plasma species). The accuracy can be improved using new Grad-Zhdanov module available in SOLPS-ITER 3.0.8 [12]. The test modeling for ITER from Ref. [13] shows that divertor compression of He with Grad-Zhdanov module improves comparing to the standard impurities description. Correspondingly, it can be expected that He concentration at the separatrix may decrease for the same source of He with this more accurate description.

3.2. Target profiles

The plasma profiles at the outer and inner divertor targets are shown in Fig. 6. Energy flux (see fig. 6e-f) includes energy fluxes of charged and neutral particles, and radiative contribution similarly to the previous paper [6]. In all cases semi-detached regime with electron temperature well below 5 eV in the strike point is observed at the outer target. The inner target is detached, but its working regime is not far from the boundary of

semi-detachment, because the far SOL region temperature rise to more than 2 eV is visible. This regime of divertor is qualitatively different from ones discussed in Ref. [4] for ITER, where both targets worked in semi-detached regime.

To stay below tungsten erosion limit electron temperature and power flux density on divertor targets must be lower than 5 eV and 5 $\frac{MW}{m^2}$, respectively [14]. Fig. 6c-f presents these parameters.

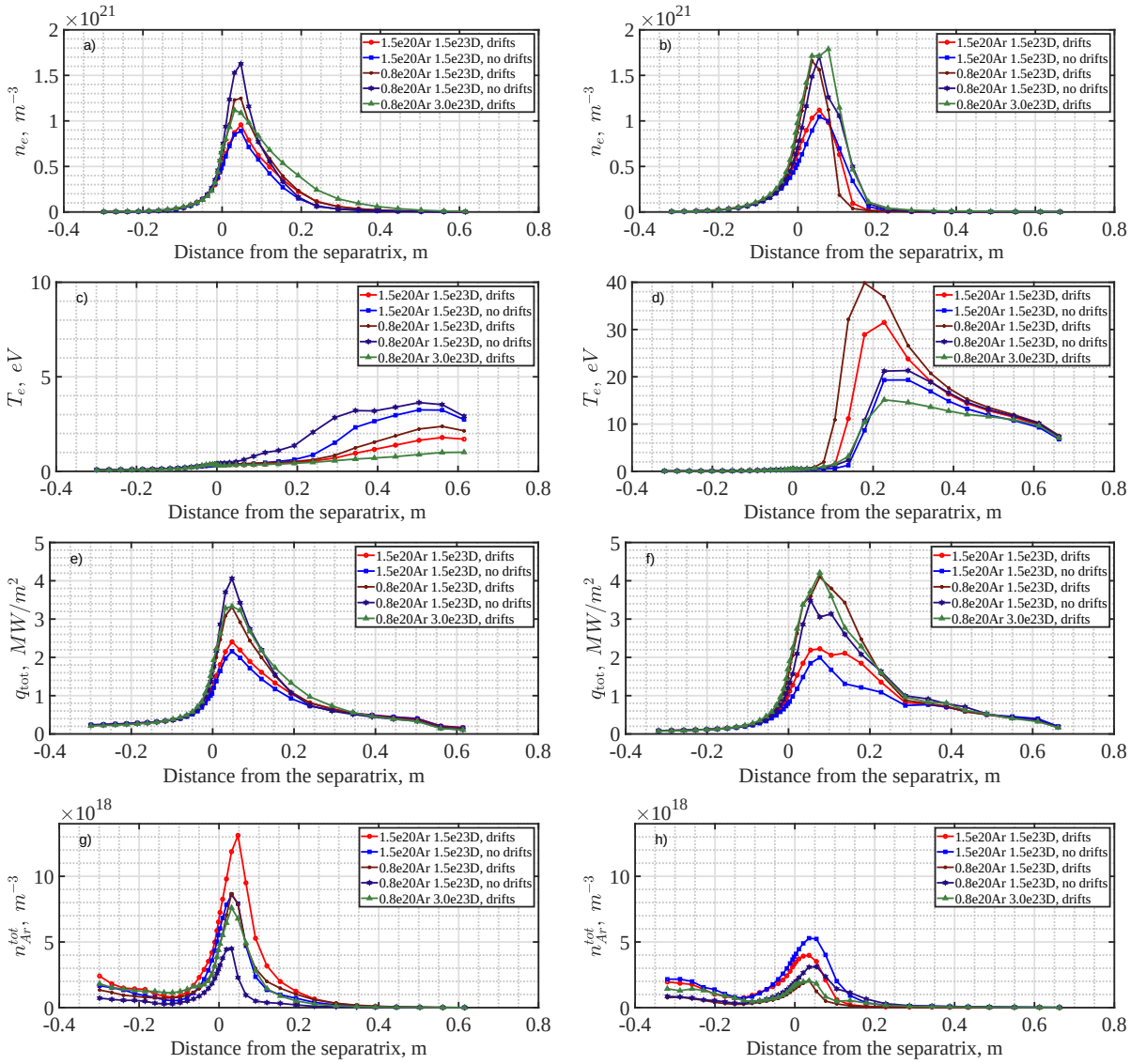

Figure 6. Plasma parameters on inner (left column) and outer (right column) divertor targets.

The heat flow towards the divertor is below the limit while temperature of the outer target far SOL remains the main problem. This problem tends to be more severe with decrease of deuterium pressure. Cases with neutral deuterium pressure $p_{D+D_2} = 10\ Pa$ and low Ar seeding have twice higher electron temperature (see fig. 6d) than the case with $p_{D+D_2} = 20\ Pa$ [6]. Comparing these runs it should be taken into account that

bigger deuterium pressure was associated in the modeling with bigger throughput, and effects of throughput and increase of the pressure can not be distinguished. In [E. Kaveeva et al, SOLPS-ITER modeling of deuterium throughput impact on the ITER SOL plasma; to be published in Journal of nuclear materials] it was shown that big throughput in case of main chamber puffing decreases the temperature in far SOL even if the pressure is kept the same by adjustement of pumping.

Peak electron temperature at outer target is almost two times higher in cases with drifts than without drifts (see fig. 6.d). This is the main effect of drifts from the point of view of targets working regime. Indeed, the outer target is deeply in semi-detached regime with almost complete dissipation of power at first 3 λ_q or more. Drifts don't play significant role in this cold region of divertor and the energy dissipation doesn't change considerably when they are turned on. The same effect was seen in Ref. [4] for ITER, where for highest seedings and power dissipation the outer target heat load was almost unchanged by turning on drifts. The drifts effect is more pronounced at the boundary of cold near SOL and hot far SOL region where both the potential variation is bigger and the solution is more sensitive to convection. Drifts lead to decrease of electrons density and impurity density in this region. The energy flow to the target increases here, but it leads more to widening of target load profile than to significant change in its maximum value. The temperature increases both due to smaller dissipation and to smaller saturation current, the latter would lead to bigger temperature even for the same heat load.

On inner divertor target the power load and electron temperature show a reverse picture. Electron temperature and power flux density are higher in cases without drifts due to the same mechanism.

Figure 7 shows flux density of tungsten sputtered from the outer target calculated by Bohdansky formula [15] without an account of prompt redesposition. The flux density from the inner target is negligible due to low enough electron temperature near the target. Tungsten flux density from outer target near the strike-point is also very low for all cases. In cases with drifts the boundary of sputtering area in the outer divertor is shifted closer to strike point together with high temperature front. Still in cases without drifts even for smaller temperature the sputtering region is wider and total sputtering is comparable to drift cases because of higher impurity presence. The limit of $\Gamma_W = 2.5 \cdot 10^{19} m^{-2} s^{-1}$ [14] for tungsten flux density sputtered from the outer target isn't exceeded only in Ar-seeded case with $p_{D+D_2} = 20\ Pa$ [6].

3.3. Impurity distribution

For each value of seeding in fig. 5b shows considerably bigger argon density both at the OMP separatrix and in the pedestal if the drifts are switched off. Taking into account almost equal outer target heat load with and without drifts for each seeding, fig. 6 f, it can be discussed as favorable effect of drifts. This result is opposite to one found in ITER modeling from Ref.[4]. The main difference between edge plasma in Ref.[4] and

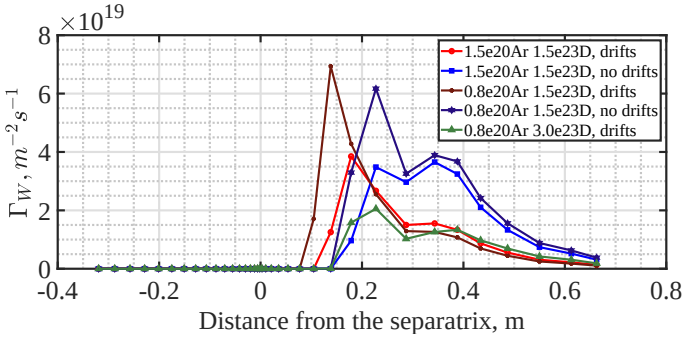

Figure 7. Tungsten flux density sputtered from the outer divertor target.

in present modeling is that in present modeling the inner divertor plasma is detached, and outer one is deep in semi-detached state fig.6c, while in Ref. [4] both divertors are in semi-detached conditions, with possibility of outer divertor re-attachment. Drifts increase the inner-outer divertor asymmetry in both cases. Still, in present modeling conditions the beneficial effect of main ions parallel flows in SOL between divertors arising due to divertors asymmetry as well as that of drift flows, both "washing out" the impurities from upstream outer SOL turns out to be more important than increase of outer target load with drifts.

One interesting feature of these regimes with detached inner target is appearance of high argon density spot ("Ar spot") in the near SOL at the inner divertor entrance, seen in fig. 8. This spot appears when the inner target cooling is sufficient, in both cases with drifts for Ar seedings $8 \cdot 10^{19} at/s$ and $1.5 \cdot 10^{20} at/s$ and in case without drifts with the bigger seeding. For Ar seeding $4 \cdot 10^{19} at/s$ the spot is absent with and without drifts. It also influences Ar density distribution at the inner midplane, fig. 5a. The Ar density maximum at the separatrix is seen there for three cases with the spot. Such Ar spot can be beneficial for formation of cold X-point solution since it can be a source of radiant in X-point region due to radial diffusion [16]. Still the modelling of cold X-point formation dynamics is needed for conclusion.

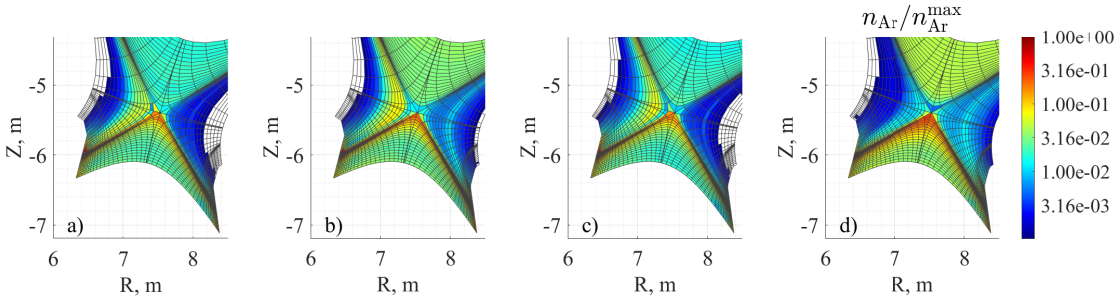

Figure 8. The ratio of argon density to the maximum argon density in the computational domain. Cases: (a) 1.5e20Ar 1.5e23D drifts on, (b) 1.5e20Ar 1.5e23D drifts off, (c) 0.8e20Ar 1.5e23D drifts on, (d) 0.8e20Ar 1.5e23D drifts off, see tabl. 1.

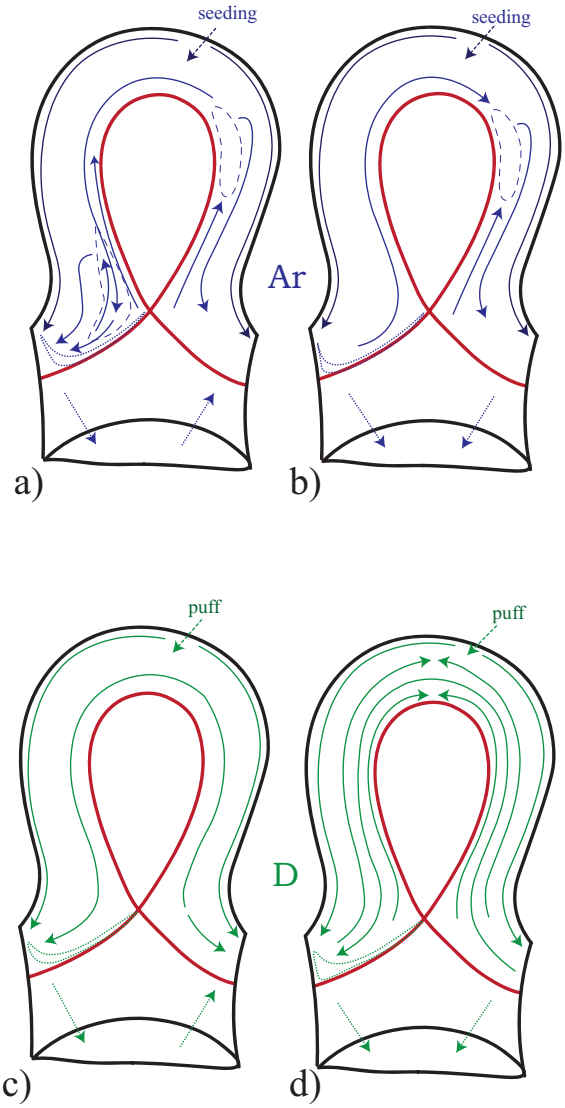

Figure 9. Argon ion (blue) and main ion (green) flux scheme in the scrape-off layer: (left column) for cases with argon spot in the HFS of the SOL, (right column) for cases without the spot. Red solid line - the separatrix. Solid arrows - ion flux, short-dashed arrows - neutral flux. Dotted line area - ionization front in the inner divertor region, dashed blue line areas - impurity accumulation.

The flow pattern analysis shows that the Ar spot generation mechanism is complex and self-consistent. Several factors should be taken into account.

i) The spot arises when ionization region both for D and Ar moves out from the inner divertor target to the distance comparable to the radial dimension of ionization zone giving much better possibility for recycling neutrals to penetrate PFR from inner divertor SOL(see dotted area in the inner divertor region on fig. 9a). This leads to increase of neutrals flow through PFR (see short-dashed arrows on fig. 9) from colder inner to hotter outer divertor and consequent ions return flow in near SOL(see solid green lines in near SOL in fig. 9c,d).

ii) The poloidal velocity of Ar ions differs from that of main ions by value, determined by thermal force [8] dragging them upstream. Combination of thermal force contribution to Ar velocity, directed upstream and main ions velocity directed downstream leads to appearance of stagnation point for poloidal velocity of Ar (see solid blue lines in near SOL in fig. 9c,d). For hotter inner divertor cases, the thermal force contribution in near SOL prevails and Ar moves towards upstream at the X-point level. Ar accumulation in the stagnation point is balanced by its radial diffusion. To facilitate the latter, big density gradient and therefore big Ar density in the stagnation point is needed. Appearance of Ar spot is accompanied by change in the integral Ar flows through the SOL. In all cases with the spot, integral parallel flow from inner to outer divertor exists. It is the biggest (10^{21} $ions/s$) for high seeding with drifts and turns out to be of the same order ($5-6\cdot10^{20}$ $ions/s$) in low seeding case with drifts and in high seeding case without drifts. In case with low seeding and without drifts, where the Ar spot is absent the Ar flow through the SOL reverses. It is smaller ($2\cdot10^{20}$ $ions/s$) by absolute value and is directed towards the outer divertor.

iii) Argon accumulation in the spot reaches the level, when $\rho_{Ar} = m_{Ar}n_{Ar}$ is of the same order with $\rho_D = m_D n_D$, so that inertia of Ar can influence the dynamics of deuterium through momentum exchange due to friction. With effective charge in the spot close to 4, electrons pressure is now affected by Ar concentration, leading to electric field change, with consequent influence on main ions. Ar accumulation also reaches the level, when the thermal force per Ar ion decreases due to its dependence on effective charge and on relative concentrations of heavy and light ions. These factors show that spot formation can not be analyzed with the same approach as less seeded SOL plasma Ref. [4], [5], [8], [10] where the poloidal velocity background for impurities is determined by main ions, while main ions distribution is affected by impurities only via energy sink due to radiation.

3.4. Radiation distribution

In EU-DEMO runs with acceptable target heat load the total radiation should reach more than 67% of power entering edge plasma, see tab. 1. In this sense these runs differ from [4] where working space of ITER corresponds to smaller radiation fraction.

Figure 10 shows distribution of radiation between different areas of the computational domain. The cases with drifts have higher total radiation in the inner divertor region than in the outer. Cases without drifts have opposite asymmetry. The figure shows total radiation losses, including deuterium and helium, but the most important radiant is Ar producing 80%-85% of total radiation.

The radiation from the SOL region and from the part of plasma inside the separatrix included into computational area (covering about 13% of total plasma area) is not negligible. About 20-30 MW is radiated from inside the separatrix. The total radiation from the core can be estimated using the coronal equilibrium approximation for radiation rate from Ref.[17]. In work [6] an effective radiation rates were calculated for Ar in EU-

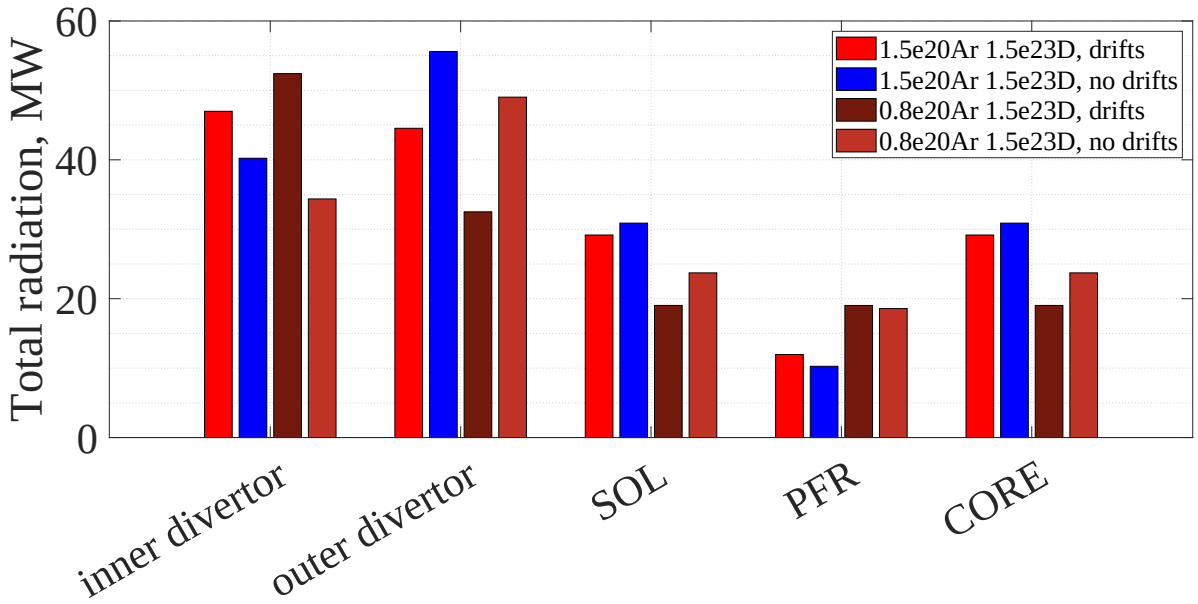

Figure 10. Total radiation of deuterium, helium and argon from each region referred to an each case. Radiation consists of line radiation, bremsstrahlung and processes, described by Eirene code.

DEMO, and it was shown that for pedestal region with temperature of 1 keV and above they are quite close the coronal equilibrium. The density and temperature distributions for EU-DEMO core plasma from Ref.[7] can be taken for estimates. They correspond to boundary plasma conditions quite close to ones obtained in present modeling and to 2 GW of fusion power. The flat Ar radial profiles in the core can be assumed, extrapolating fig. 5. This estimate gives up to $P_{rad} = 145\ MW$ in a case with $c_{Ar} = 0.6\%$ and $P_{rad} = 200\ MW$ in a case with $c_{Ar} = 0.9\%$.

This indicates that fusion power relevant to the regimes of divertor discussed above should be bigger than 1 GW but it's still below the expected 2 GW working regime. In the latter regime the helium exhaust should be twice bigger. Still the helium concentration at the separatrix taken from table 1 and scaled with coefficient two remains below the limit. Calculations show that helium radiation from inside the separatrix is negligible and it's radiation from the divertor and the SOL in present modeling is about 1 MW or less. Therefore additional exhaust of He won't change the main patterns of the solution.

4. Conclusions

EU-DEMO edge modeling was performed for regimes with 1-2 GW of fusion power (200 MW of power in edge plasma) and the moderate divertor neutrals pressure 10 Pa. Ar seeding was used for divertor dissipation. Full description of drifts and kinetic neutrals is included in the modeling. It is shown that highly radiating regimes with power dissipation of approximately 70% in the divertor and SOL are attainable for Ar

concentration at separatrix below 1%. These regimes meet the condition of outer target heat load below 5 MW/m^2. Still, the temperature in far SOL is too big and tungsten sputtering can exceed the acceptable limit.

The effect of drifts was analyzed by reproducing the same runs with drifts turned off. In these highly radiating regimes turning off drift effects leads to (a) considerable decrease of outer target electron temperature, (b) increase of both intrinsic (He) and seeded (Ar) impurity density in the pedestal. The effect of drifts on total dissipation and maximal target load is moderate.

The change of impurities spatial distribution is observed with transition of inner target to detachment. Cooling of inner divertor below certain threshold soon after detachment of inner target leads to appearance of Ar spot in the inner SOL near X-point. The mechanism of spot formation is independent on drifts, but associated with increase of asymmetry between outer and inner divertor.

5. Acknowledgments

This work was supported by Russian Science Foundation, grant no. NNN ???. Numerical calculations were performed at the Polytechnic Supercomputer Center at Peter the Great St. Petersburg Polytechnic University.

References

1. Federici, G. *et al.* Overview of the DEMO staged design approach in Europe. *Nuclear Fusion* **59.** ISSN: 17414326 (6 Apr. 2019).
2. Subba, F., Coster, D. P., Moscheni, M. & Siccinio, M. SOLPS-ITER modeling of divertor scenarios for EU-DEMO. *Nuclear Fusion* **61.** ISSN: 17414326 (10 Oct. 2021).
3. Aho-Mantila, L. *et al.* Predictions of radiation pattern and in-out asymmetries in the DEMO scrape-off layer using fluid neutrals. *Nuclear Fusion* **62.** ISSN: 17414326 (5 May 2022).
4. Kaveeva, E. *et al.* SOLPS-ITER modelling of ITER edge plasma with drifts and currents. *Nuclear Fusion* **60.** ISSN: 17414326 (4 2020).
5. Rozhansky, V. *et al. Multi-machine SOLPS-ITER comparison of impurity seeded H-mode radiative divertor regimes with metal walls* (2021).
6. Vekshina, E. *et al.* SOLPS-ITER EU-DEMO modelling with drifts and kinetic neutrals. *Contributions to Plasma Physics* **62.** ISSN: 15213986 (5-6 June 2022).
7. Siccinio, M. *et al.* DEMO physics challenges beyond ITER. *Fusion Engineering and Design* **156.** ISSN: 09203796 (July 2020).
8. Senichenkov, I. Y. *et al.* On mechanisms of impurity leakage and retention in the tokamak divertor. *Plasma Physics and Controlled Fusion* **61.** ISSN: 13616587 (2019).

9. Eich, T., Goldston, R. J., Kallenbach, A., Sieglin, B. & Sun, H. J. Correlation of the tokamak H-mode density limit with ballooning stability at the separatrix. *Nuclear Fusion* **58.** ISSN: 17414326 (3 Jan. 2018).
10. Pitts, R. A. *et al. Physics basis for the first ITER tungsten divertor* Aug. 2019.
11. Dunne, M. G. *et al.* The role of the density profile in the ASDEX-Upgrade pedestal structure. *Plasma Physics and Controlled Fusion* **59.** ISSN: 13616587 (1 Jan. 2017).
12. Makarov, S. O. *et al.* Equations and improved coefficients for parallel transport in multicomponent collisional plasmas: Method and application for tokamak modeling. *Physics of Plasmas* **28.** ISSN: 10897674 (6 June 2021).
13. Makarov, S. O. *et al.* Impact of the improved parallel kinetic coefficients on the helium and neon transport in SOLPS-ITER for ITER. *Contributions to Plasma Physics* **62.** ISSN: 15213986 (5-6 June 2022).
14. Kallenbach, A. *et al. Impurity seeding for tokamak power exhaust: from present devices via ITER to DEMO* (Dec. 2013).
15. Bohdansky, J. A universal relation for the sputtering yield of monatomic solids at normal ion incidence. *Nuclear Instruments and Methods in Physics Research* **2.** ISSN: 17414326 (1-3 Mar. 1984).
16. Reimold, F. *et al.* The high field side high density region in SOLPS-modeling of nitrogen-seeded H-modes in ASDEX Upgrade. *Nuclear Materials and Energy* **12,** 193–199. ISSN: 23521791 (Aug. 2017).
17. Mavrin, A. A. Radiative Cooling Rates for Low-Z Impurities in Non-coronal Equilibrium State. *Journal of Fusion Energy* **36,** 161–172. ISSN: 01640313 (4-5 Oct. 2017).